# Kinetic Study of the Equilibrium $HO_2 + NO \rightleftarrows OH + NO_2$ and the Thermochemistry of $HO_2$

**Carleton J. Howard**

*Contribution from the Aeronomy Laboratory, NOAA/Environmental Research Laboratories, Boulder, Colorado 80303.* *Received May 2, 1980*

**Abstract:** Rate constants for the reactions $HO_2 + NO \rightarrow OH + NO_2$ ($k_F$) and $OH + NO_2 \rightarrow HO_2 + NO$ ($k_R$) have been measured at high temperatures by using laser magnetic resonance detection of $HO_2$ and OH reactants in a flow tube reactor. The results are $k_F(T) = (3.51 \pm 0.35) \times 10^{-12} \exp[(+240 \pm 30)/T]$ cm$^3$ molecule$^{-1}$ s$^{-1}$ for $232 < T < 1271$ K, including earlier low-temperature measurements and $k_R(T) = (3.03 \pm 0.60) \times 10^{-11} \exp[-(3360 \pm 125)/T]$ cm$^3$ molecule$^{-1}$ s$^{-1}$ for $452 < T < 1115$ K. These data are combined with other thermochemical data to calculate the heat of formation of the $HO_2$ radical, $\Delta H_f°_{298} = 2.5 \pm 0.6$ kcal mol$^{-1}$. Other measurements of this quantity and the thermochemistry of $HO_2$ are discussed.

## 1. Introduction

The hydroperoxyl radical, $HO_2$, is an important intermediate in atmospheric chemistry,[1] in combustion,[2] and in most chain-reaction mechanisms involving oxidation of molecules which contain hydrogen. Its thermochemistry, specifically the heat of formation, $\Delta H_f°$,[3] is a critical factor in evaluating possible reactions of $HO_2$ in the atmosphere because reactions that are endothermic by more than about 3 kcal mol$^{-1}$ are usually too slow to be significant. Similarly, in combustion, thermochemical data are the basis for evaluating initiation mechanisms, branching ratios, and equilibrium constants.

The currently accepted value of the heat of formation of $HO_2$,[4] $\Delta H_f°_{298}(HO_2) = 5 \pm 2$ kcal mol$^{-1}$, is based upon data from the classic study of Foner and Hudson,[5] who used electron-impact ionization with a modulated molecular beam mass spectrometer. Recently Kochubei and Moin[6] have challenged the accuracy of this value, and from kinetic studies of the temperature dependence of reaction 1, where X = Cl, Br, or I, they have deduced

$$HX + O_2 \rightarrow HO_2 + X \qquad (1)$$

$\Delta H_f°_{298}(HO_2) = 0.9$ kcal mol$^{-1}$. The maximum difference between these two measurements including the uncertainty in each is about 8 kcal mol$^{-1}$. This large range of values does not allow a definitive assessment of the likelihood of several important atmospheric $HO_2$ reactions such as eq 2, 3, and 4. If one assumes $\Delta H_f°(HO_2) =$

$$HO_2 + NO \rightarrow HNO + O_2 \qquad (2)$$

$$HO_2 + ClO \rightarrow ClOO + OH \qquad (3)$$

$$HO_2 + Cl \rightarrow ClO + OH \qquad (4)$$

$\Delta H_f°(HO_2) = 0.9$ kcal mol$^{-1}$, reactions 2-4 are endothermic by 1.3, 5.3, and 3.8 kcal mol$^{-1}$, respectively. If on the other hand, $\Delta H_f°(HO_2) = 5.0$ kcal mol$^{-1}$, then reactions 2 and 4 are exothermic and (3) is only slightly endothermic ($\sim 1.2$ kcal mol$^{-1}$).

In this work the value of $\Delta H_f°(HO_2)$ is determined from measurements of the temperature dependence of the rate constants for the forward and reverse reactions

$$HO_2 + NO \rightleftarrows OH + NO_2$$

The equilibrium constant $K_e = k(\text{forward})/k(\text{reverse})$ is combined with thermodynamic data, $\Delta H_f°$ and $S°$, for NO, OH, and $NO_2$ to obtain $\Delta H_f°(HO_2)$. The standard entropy of $HO_2$ is also reevaluated by using new spectroscopic data.

## 2. Experimental Section

The kinetic measurements are made by using a discharge-flow reactor coupled with a water-vapor laser magnetic resonance (LMR) spectrometer for detection of $HO_2$, OH, NO, and $NO_2$. A detailed description of the apparatus[7] and a recent low-temperature study of the forward ($HO_2 + NO$) reaction[8] are published. Only a brief description of the measurement techniques is given here.

The LMR spectrometer is used to detect paramagnetic radicals with rotational transitions that are nearly coincident with the laser wavelength, in this case $\lambda = 118.6$ $\mu$m. Resonant absorption of the laser radiation is achieved by passing the radicals through the laser cavity and by Zeeman tuning a component of the rotational transition to the fixed laser frequency. When the radicals absorb the laser radiation, their concentration is proportional to the fractional change in the laser output power. Some aspects of the LMR spectroscopy of $HO_2$,[9] NO,[10] OH,[11] and $NO_2$[12] are described in previous publications. The method is sensitive and specific for the detection of the ground vibrational and electronic states.

A special high-temperature flow reactor designed for this work is shown in Figure 1. The quartz flow tube is 25.0-mm i.d. and about 102 cm long. The He carrier gas (≥99.999% purity) enters the tube near the top. The $HO_2$ radicals are made in a high-pressure source[8] ($p \simeq 20$ torr) by the reaction $H + O_2 + M \rightarrow HO_2 + M$ ($k = 5 \times 10^{-32}$ cm$^6$ molecule$^{-2}$ s$^{-1}$).[13] OH radicals are made in the flow tube by the reaction $H + NO_2 \rightarrow OH + NO$ ($k = 1.4 \times 10^{-10}$ cm$^3$ molecule$^{-1}$ s$^{-1}$).[14] The reactant, $HO_2$ or OH, mixes with the carrier gas and enters a 60-cm long section of the flow tube that is surrounded by a furnace. The furnace consists of a No. 24 strand of nichrome wire wrapped uniformly with about 8-mm spacing around the flow tube. Thermal insulation is provided by (a) 3 layers of 1.6-mm thick asbestos tape, (b) 4 layers of alternate Al foil and 1.6-mm thick glass cloth, and (c) a 6-mm layer of glass braid. The gas stream flows about 10 cm in the temperature controlled region before it reaches the first of 6 reactant gas ports spaced at 7-cm intervals. Each port is attached by stainless-steel tubing to a valve connected to a manifold that supplies the NO or $NO_2$ reactant. The reaction begins at the point of addition of this reactant to the gas stream and continues to the detection region at the bottom of the flow tube. The detection region is located at the intersection of the flow tube and the laser cavity. It is defined by the homogeneous magnetic field indicated by the dashed circle on Figure 1. A stream of $N_2$ is injected into the laser tube to flush the reactants

(1) Duewer, W. H.; Wuebbles, D. J.; Ellsaesser, H. W.; Chang, J. S. *JGR, J Geophys. Res.* **1977**, *82*, 935-942.
(2) Benson, S. W.; Nangia, P. S. *Acc. Chem. Res.* **1979**, *12*, 223-228.
(3) Throughout this paper the standard state for thermochemical data is 298 K and 1 atm unless otherwise noted. Bond dissociation energies refer to the $\Delta H°_{298}$ for the reaction which breaks the indicated bond, e.g., $D(H-O_2) = \Delta H_f°_{298}(HO_2) - \Delta H_f°_{298}(H) - \Delta H_f°_{298}(O_2)$. All thermochemical data from JANAF.[4]
(4) Stull, D. R., Prophet, H., Eds., "JANAF Thermochemical Tables"; National Bureau of Standards: Washington, D.C.; compiled and calculated by the Dow Chemical Co., Midland, MI, including revised tables issued through 1979.
(5) Foner, S. N.; Hudson, R. L. *J. Chem. Phys.* **1962**, *36*, 2681-2688 and references cited therein.
(6) Kochubei, V. F.; Moin, F. B. *Dokl. Akad. Nauk SSSR* **1974**, *219*, 141-144.
(7) Howard, C. J.; Evenson, K. M. *J. Chem. Phys.* **1974**, *61*, 1943-1952.
(8) Howard, C. J. *J. Chem. Phys.* **1979**, *71*, 2352-2359.
(9) Hougen, J. T.; Radford, H. E.; Evenson, K. M.; Howard, C. J. *J. Mol. Spectrosc.* **1975**, *56*, 210-228.
(10) Mizushima, M.; Evenson, K. M.; Wells, J. S. *Phys. Rev. A* **1972**, *5*, 2276-2287.
(11) Evenson, K. M.; Wells, J. S.; Radford, H. E. *Phys. Rev. Lett.* **1970**, *25*, 199-202.
(12) Curl, R. F., Jr.; Evenson, K. M.; Wells, J. S. *J. Chem. Phys.* **1972**, *56*, 5143-5151.
(13) Kurylo, M. J. *J. Phys. Chem.* **1972**, *76*, 3518-3526.
(14) Michael, J. V.; Nava, D. F.; Payne, W. A.; Lee, J. H.; Stief, L. J. *J. Phys. Chem.* **1979**, *83*, 2818-2823.

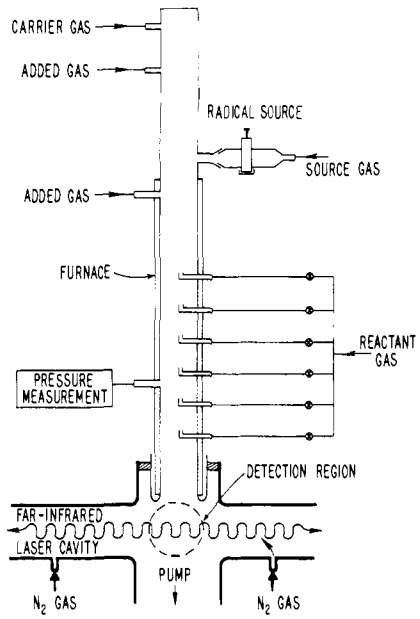


Figure 1. Schematic of high-temperature flow-tube reactor.

from the laser cavity. The usual moveable inlet method of reactant addition could not be used at high temperatures because the lubricant coating on the inlet reacts at high temperatures with $O_2$ and $NO_2$ to generate large concentrations of radicals.

The flow-tube pressure is measured with a capacitance manometer (±1% accuracy) near the center of the reaction zone.

The flow-tube temperature is measured with three chromel–alumel thermocouples located on the quartz tube about 7, 32, and 56 cm from the bottom of the furnace. The digital temperature readout was calibrated with an ice point compensated microvolt potentiometer by using NBS tables[15] and found to be accurate to within the resolution of the thermometer (±1 °C) over the range 300–1300 K. The temperature profile along the flow-tube axis was measured with a thermocouple attached to a quartz rod and is uniform (±5 °C) along the middle 45-cm section of the reactor.

Although normally either $H_3BO_3$ or $H_3PO_4$ coatings are applied to the flow-tube interior to inhibit OH and $HO_2$ wall destruction, they cannot be used here because they are pyrolyzed at high temperatures. The flow-tube surface was conditioned by flowing high concentrations of OH, $\simeq 5 \times 10^{12}$ molecule cm$^{-3}$, and $O_2$, $\simeq 5 \times 10^{16}$ molecule cm$^{-3}$, through the tube for several hours at $T \simeq 1200$ K. After this treatment the first-order wall reaction rate constant for both OH and $HO_2$ is small, <10 s$^{-1}$. The $k_w$(OH) was measured by adding a small concentration of $NO_2$ ($\leq 10^{11}$ molecule cm$^{-3}$) through the different inlet ports to a large concentration of H ($\simeq 10^{13}$ atom cm$^{-3}$). The $k_w(HO_2)$ was estimated by measuring the change in OH concentration that results from adding an excess of NO ($\simeq 10^{14}$ molecule cm$^{-3}$) through different inlet ports to a stream containing $HO_2$. It was also estimated by measuring the change in $HO_2$ concentration with a fixed $HO_2$ source and different flow velocities. The small values observed for $k_w$ are typical for a well conditioned 2.5-cm diameter flow tube. The rate constant analysis assumes that $k_w$ does not change upon addition of NO or $NO_2$ reactant.

The NO reactant was purified by passing it through a silica gel trap cooled with dry ice. The $NO_2$ reactant was prepared from purified NO by reaction with excess $O_2$ at a pressure of about 1200 torr. The $NO_2$ was stored under about 500 torr of $O_2$ in a glass reservoir with a Teflon valve. LMR analysis of the $NO_2$ reactant indicated <0.2% NO impurity in the flow tube. A small flow of He ($\simeq 0.5$ STP cm$^3$ s$^{-1}$) was added to the NO and $NO_2$ reactant flows to flush them through the inlet lines.

The typical experimental conditions are as follows: flow velocity, $\bar{v}$ = 900–4300 cm s$^{-1}$; [M] = [He] + [$O_2$] = (1–5.3) × $10^{16}$ molecule cm$^{-3}$; $[OH]_0$ = (3–10) × $10^{10}$ molecule cm$^{-3}$; $[HO_2]_0$ = (8–15) × $10^{10}$ molecule cm$^{-3}$; [NO] = (5–32) × $10^{12}$ molecule cm$^{-3}$; and $[NO_2]$ = (1.6–150) × $10^{13}$ molecule cm$^{-3}$. Under these conditions, the reactions are pseudo first order in OH or $HO_2$. Rate constants are obtained from plots of the relative concentration of OH or $HO_2$ as a function of $z$, the distance from the bottom of the flow tube to the reactant inlet ports. The first-order rate constant is given by the slope of a plot of ln [$A$] vs. $z/\bar{v}$, where $A$ = OH or $HO_2$ and $\bar{v}$ is the average flow velocity. The standard error (1 $\sigma$) derived from fitting these plots was typically between 1.5 and 5%. The second-order rate constant is given by dividing the first-order rate constant by the reactant concentration, [NO] or [$NO_2$]. As a test for possible interference from wall reactions, all the data (3 to 6 points) for a single temperature were plotted, first-order rate constant vs. reactant concentration. The slopes of these plots are second-order rate constants that agreed very well with the values obtained by averaging the individual second-order rate constants. Least-squares fits to these plots gave intercepts which were randomly distributed around the origin. The intercepts were usually within 1 $\sigma$ of the origin and, with only a couple exceptions, always within the 95% confidence range. Each decay plot was taken as a kinetic measurement in the subsequent fitting to obtain the temperature dependence.

An analysis of the single kinetic measurement precision given by the measurement of the gas-flow rates (±3%), temperature (±1%), pressure (±1%), flow tube radius (±1%), and the slope of the decay plots (±4%) gives a value of about 8.5%. This can be compared with the standard deviation of the residuals (1 $\sigma$) calculated for the average of each second-order measurement set or for the slope of the first-order rate constant vs. reactant concentration plots. For the $HO_2$ + NO reaction data the measurement precision is about 5%, and for the OH + $NO_2$ reaction it is about 8%. The measurement precision may be poorer for the OH + $NO_2$ reaction because of the difficulty in measuring the $NO_2$ flow rate, the tendency for $NO_2$ to decompose slightly at high temperatures or the much larger temperature dependence of that reaction.

Table I. Summary of Rate Constant Measurements for the Forward Reaction $HO_2$ + NO

| no. of expt | [M], $10^{16}$ molecule cm$^{-3}$ | $\bar{v}$, cm s$^{-1}$ | [NO] range, $10^{12}$ molecule cm$^{-3}$ | $k_F \pm \sigma$,[a] $10^{-12}$ cm$^3$ molecule$^{-1}$ s$^{-1}$ | $T$, K |
|---|---|---|---|---|---|
| 4 | 1.61 | 3620 | 15.1–37.7 | 4.87 ± 0.24 | 793 |
| 6 | 1.05 | 4320 | 23.9–55.0 | 4.28 ± 0.32 | 1043 |
| 7 | 1.13 | 4020 | 22.3–57.6 | 5.24 ± 0.26 | 968 |
| 5 | 1.88 | 3540 | 11.0–27.6 | 4.30 ± 0.22 | 833 |
| 7 | 3.37 | 2280 | 5.17–21.0 | 6.01 ± 0.32 | 493 |
| 3 | 2.35 | 3430 | 7.60–18.5 | 4.33 ± 0.19 | 1271 |
| 3 | 2.47 | 3240 | 7.02–15.0 | 4.21 ± 0.09 | 1198 |
| 3 | 3.41 | 2230 | 13.9–26.7 | 5.47 ± 0.26 | 461 |
| 3 | 3.32 | 2270 | 5.70–17.0 | 5.85 ± 0.16 | 471 |
| 4 | 2.62 | 2860 | 7.73–31.0 | 5.72 ± 0.26 | 608 |
| 4 | 2.99 | 1980 | 6.72–26.9 | 6.16 ± 0.37 | 423 |
| 4 | 2.40 | 2450 | 7.55–27.1 | 5.75 ± 0.37 | 538 |
| 4 | 2.27 | 2600 | 7.64–29.7 | 5.24 ± 0.27 | 575 |
| 4 | 2.05 | 2900 | 7.63–31.3 | 4.91 ± 0.09 | 651 |
| 4 | 2.52 | 2360 | 8.27–22.7 | 4.53 ± 0.13 | 739 |
| 4 | 2.04 | 2890 | 6.67–22.2 | 4.46 ± 0.25 | 925 |

[a] $\sigma$ = calculated standard deviation of the residuals.

## 3. Results

The $HO_2$ + NO kinetic measurements are summarized in Table I. A total of 69 individual measurements of $k_F$ were made at 16 different temperatures between 423 and 1271 K. Also shown in Table I are the total gas density, [M], the flow velocity, $\bar{v}$, and the range of the reactant concentration [NO] for each experimental set. The values given for $k_F$ are the average of 3–7 individual measurements and the standard error (±1 $\sigma$). A correction (<4%) for axial diffusion is applied to the data.[16]

The data for $k_F$ (69 points) were fit to an Arrhenius expression to give $k_F(T) = (3.57 \pm 0.23) \times 10^{-12} \exp[(226 \pm 41)/T]$ cm$^3$ molecule$^{-1}$ s$^{-1}$, where the error limits represent the statistical 95% confidence limits. Alternatively, either the slopes of the first-order rate constants vs. [NO] plots or the average values of $k_F$ given in Table I can also be fitted. For example, the fit to the average values in Table I gave $k_F(T) = (3.54 \pm 0.41) \times 10^{-12} \exp[(230 \pm 72)/T]$ cm$^3$ molecule$^{-1}$ s$^{-1}$, where the errors are 95% confidence limits. The major difference between these two results is the magnitude of the error limits which reflects the difference in the

(15) Powell, R. L.; Hall, W. J.; Hyink, C. H., Jr.; Sparks, L. L.; Burns, G. W.; Scroger, M. G.; Plumb, H. H. *NBS Monogr.* **1974**, *No. 125*, 137–152.

(16) The axial diffusion correction is made by multiplying the measured second-order rate constant by $(1 + k^1D/\bar{v}^2)$, where $k^1$ is the observed first-order rate constant (s$^{-1}$), $D$ is the diffusion constant for the radical in the carrier gas (cm$^2$ s$^{-1}$), and $\bar{v}$ is the flow velocity, (cm s$^{-1}$): Kaufman, F. *Prog. React. Kinet.* **1961**, *1*, 3–39. Diffusion coefficients are estimated, $Dp$(OH-He) = 3.42 × $10^{-2}T^{1.72}$ cm$^2$ torr s$^{-1}$, $Dp(HO_2$–He) = 3.20 × $10^{-2}T^{1.72}$ cm$^2$ torr s$^{-1}$, and $Dp(HO_2$–$O_2)$ = 8.10 × $10^{-3}T^{1.72}$ cm$^2$ torr s$^{-1}$: Marrero, T. R.; Mason, E. A. *J. Phys. Chem. Ref. Data* **1972**, *1*, 3–118.

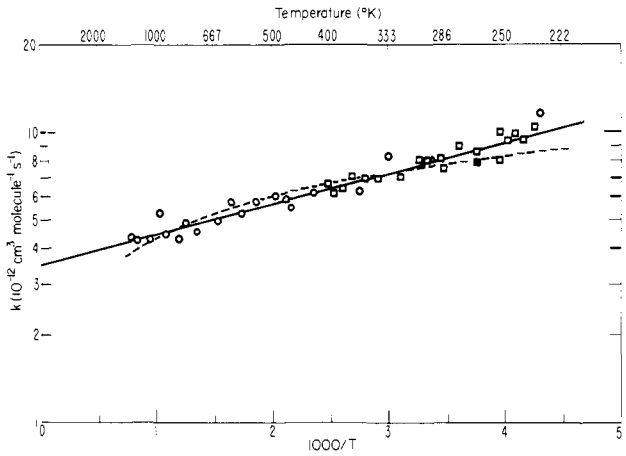


**Figure 2.** Summary of data on the temperature dependence of $k_F(HO_2 + NO)$: (○) this work, $423 < T < 1271$ K; (□) ref 8, $232 < T < 403$ K. The solid line is the fit given by $k_F(T) = (3.51 \pm 0.13) \times 10^{-12} \exp[(240 \pm 16)/T]$ cm$^3$ molecule$^{-1}$ s$^{-1}$. The dashed line is given by $k_F(T) = (1.11 \pm 0.15) \times 10^{-10} T^{-0.47 \pm 0.04}$ cm$^3$ molecule$^{-1}$ s$^{-1}$. Each point in this figure is obtained by averaging 3–7 individual measurements at a single temperature. The fits are made to the complete data set as described in text.

number of degrees of freedom of the fits (number of data points minus 2). Since the first set has about 4 times as many data points, the standard errors on that fit are about $1/n^{1/2} \approx {}^1/_2$. The preference for using the complete set instead of the averages for fitting is based on the interpretation that each rate constant, i.e., decay plot, constitutes a measurement and that the Arrhenius coefficient error limits derived from fitting these data more accurately reflect the random errors of the complete measurement set.

The Arrhenius expression for the high-temperature data given above agrees very well with the previously published[8] result for the temperature range $232 < T < 403$ K, $k_F(T) = (3.3 \pm 0.7) \times 10^{-12} \exp[(254 \pm 50)/T]$ cm$^3$ molecule$^{-1}$ s$^{-1}$. Therefore, the two sets of data are combined as shown in Figure 2, and a fit to the complete set yields $k_F(T) = (3.51 \pm 0.13) \times 10^{-12} \exp[(240 \pm 16)/T]$ cm$^3$ molecule$^{-1}$ s$^{-1}$ for the range $232 < T < 1271$ K with the 95% confidence limits of the fit. Including an estimate of possible systematic errors gives $k_F(T) = (3.51 \pm 0.35) \times 10^{-12} \exp[(240 \pm 30)/T]$ cm$^3$ molecule$^{-1}$ s$^{-1}$. These data are also fit to a $T^n$ expression as indicated by the dashed line in Figure 2. The result is $k_F(T) = (7.6 \pm 0.25) \times 10^{-12}(T/300)^{-0.47 \pm 0.04} = (1.11 \pm 0.15) \times 10^{-10} T^{-0.47 \pm 0.04}$ cm$^3$ molecule$^{-1}$ s$^{-1}$, with 95% confidence limits. This can be compared with $(7.9 \pm 1.0) \times 10^{-12}(T/300)^{-0.83 \pm 0.18}$ obtained in fitting the low-temperature set.[8] The latter value includes an estimate of systematic errors. By fitting to data covering a large temperature range, it was possible to distinguish between the quality of fit obtained with the Arrhenius and the $T^n$ models. The Arrhenius model is preferred for the following reasons: (1) the variance of the residuals for the $T^n$ fit was about 50% larger than that for the Arrhenius fit, (2) the standard deviations of the predicted rate constants for the $T^n$ model were significantly larger, about 40% at 1271 K, 20% at 739 K, and roughly equal at 232 K, and finally (3) a plot of the residuals vs. temperature showed a normal distribution for the Arrhenius fit but was curved for the $T^n$ fit. The latter difference also can be seen in Figure 2 where the $T^n$ model curve falls below the data set at the temperature extrema.

The data for the reverse reaction $k_R(OH + NO_2)$ are summarized in Table II. There are 43 individual measurements at 10 different temperatures between 452 and 1115 K. The carrier gas density, flow velocity, and the range of $[NO_2]$ are also shown for each set in Table II. The data are also corrected for axial diffusion (<12%).[16] The data at 702 K and lower temperatures include an additional correction for the competing reaction (5).

$$OH + NO_2 + He \rightarrow HNO_3 + He \qquad (5)$$

The temperature dependence of the rate constant $k_5$ has been

**Table II.** Summary of Rate Constant Measurements for the Reverse Reaction $OH + NO_2$

| no. of expt | [M], $10^{16}$ molecule cm$^{-3}$ | $\bar{v}$, cm s$^{-1}$ | $[NO_2]$ range, $10^{13}$ molecule, cm$^{-3}$ | $k_R \pm \sigma$,[a] $10^{-14}$ cm$^3$ molecule$^{-1}$ s$^{-1}$ | $T$, K |
|---|---|---|---|---|---|
| 4 | 1.73 | 1770 | 1.58–7.09 | 154 ± 9.2 | 1115 |
| 4 | 2.87 | 1070 | 3.76–20.6 | 24.9 ± 3.0 | 702 |
| 4 | 2.49 | 1260 | 2.76–8.06 | 133 ± 14 | 1028 |
| 6 | 2.98 | 1050 | 3.34–12.8 | 68.0 ± 2.9 | 868 |
| 4 | 4.23 | 754 | 12.0–33.1 | 14.3 ± 1.2 | 625 |
| 4 | 5.27 | 603 | 18.6–46.5 | 3.84 ± 0.30 | 504 |
| 4 | 1.78 | 1720 | 73.4–143 | 2.02 ± 0.12 | 452 |
| 4 | 1.47 | 2060 | 36.7–106 | 6.28 ± 0.35 | 546 |
| 4 | 1.02 | 2880 | 12.6–47.3 | 44.3 ± 7.3 | 785 |
| 5 | 3.28 | 922 | 4.93–19.3 | 36.7 ± 2.0 | 786 |

[a] $\sigma$ = calculated standard deviation of the residuals.

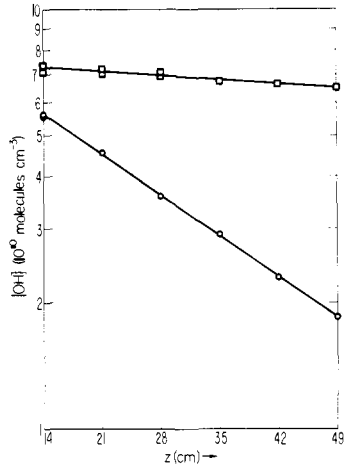


**Figure 3.** OH + $NO_2$ decay plots: $T = 546$ K, $\bar{v} = 2082$ cm s$^{-1}$, [He] $= 1.49 \times 10^{16}$ molecule cm$^{-3}$, $[NO_2] = 1.06 \times 10^{15}$ molecule cm$^{-3}$, (○) [NO] = 0, (□) [NO] $= 2.6 \times 10^{14}$ molecule cm$^{-3}$. The steep decay is due to (a) $OH + NO_2 \rightarrow HO_2 + NO$ and (b) $OH + NO_2 + He \rightarrow HNO_3 + He$, and the small decay is due to only (b). The rate constant for (a), $k_R$, is obtained by subtracting the small decay constant from the steep decay constant.

measured by Anderson et al.[17] and Anastasi and Smith,[18] who report $k_5 \simeq 1 \times 10^{-30}(T/300)^{-2.5}$ cm$^6$ molecule$^{-2}$ s$^{-1}$. The effect of reaction 5 was measured directly by adding a large concentration of NO to the flow tube. NO reacts with the $HO_2$ product of the $OH + NO_2$ reaction, regenerating OH, and the resultant decrease in OH is due to reaction 5. This is illustrated in Figure 3 which shows two sets of OH decay plots: (□) with added NO and (○) without added NO. The rate constant calculated from the data with NO added is subtracted from the rate constant calculated from the data obtained without NO. The difference is $k_R$. This correction was largest at the lowest temperatures and highest pressures. The largest correction (≃25%) was applied to the data at 504 K.

The failure to observe any reaction when large concentrations of both NO and $NO_2$ are present in the flow tube at $T > 702$ K is taken as an indication that there are no competing channels such as reaction 2. All such reactions would irreversibly remove radicals and would cause a decline in the OH and $HO_2$ concentrations. The limit placed on all competing channels is <10%. This conclusion is further supported by the direct observation of the formation of OH from $HO_2 + NO$ and the formation of $HO_2$ from $OH + NO_2$.

The measurements of the reverse rate constant are shown in Arrhenius form in Figure 4. They vary over almost two decades for the range $452 < T < 1115$ K. The line shows the fit given

(17) Anderson, J. G.; Margitan, J. J.; Kaufman, F. *J. Chem. Phys.* **1974**, *60*, 3310–3317.
(18) Anastasi, C.; Smith, I. W. M. *J. Chem. Soc., Faraday Trans. 2* **1976**, *72*, 1459–1468.

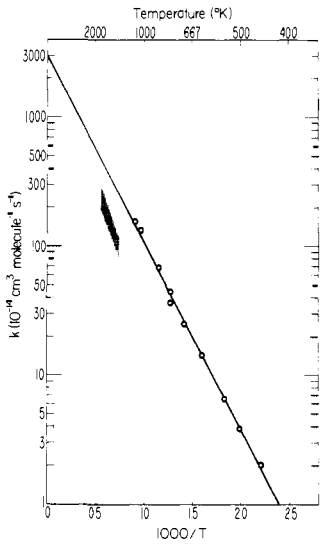


**Figure 4.** Arrhenius plot of the data for $k_R(OH + NO_2)$. Each point is the average of 4–6 individual measurements at a single temperature. The fit $k_R(T) = (3.03 \pm 0.41) \times 10^{-11} \exp[-(3360 \pm 93)/T]$ cm$^3$ molecule$^{-1}$ s$^{-1}$ is obtained with the complete set. The shaded area represents the measurements of Glänzer and Troe[22] described in the text.

by $k_R(T) = (3.03 \pm 0.41) \times 10^{-11} \exp[-(3356 \pm 93)/T]$ cm$^3$ molecule$^{-1}$ s$^{-1}$, where the error limits indicate the 95% confidence limits. Including an estimate of possible systematic errors gives $k_R(T) = (3.03 \pm 0.60) \times 10^{-11} \exp[-(3356 \pm 125)/T]$.

The measured rate constants for the forward and reverse reaction can be combined to give the temperature-dependent equilibrium constant $K_e = k_F/k_R = (0.116 \pm 0.026) \exp[-(7145 \pm 255)/RT]$. The valid temperature range for this result is 452–1115 K. The temperature dependence of the equilibrium constant is given by the solid line in Figure 5.

Two different methods are used to obtain $\Delta H_f°(HO_2)$ from the equilibrium constant data. The first method is a second-law calculation in which the heat of reaction ($\Delta H_r$) is taken as the slope of the van't Hoff plot. Thus, $\Delta H_r°_{700} = -7145 \pm 255$ cal mol$^{-1}$ and $\Delta H_f°_{700}(HO_2) = \Delta H_f°_{700}(OH) + \Delta H_f°_{700}(NO_2) - \Delta H_f°_{700}(NO) - \Delta H_r°_{700}$. Second-law values of $\Delta H_f°_{298}(HO_2)$ are calculated by using reference thermochemical data from two different sources: ref 4 (JANAF) and 19 (TPIS). The results are $\Delta H_f°_{298} = 3.0$ (JANAF) and 3.1 (TPIS) kcal mol$^{-1}$.

The second and preferred method of obtaining $\Delta H_f°_{298}(HO_2)$ is a third-law calculation. In this case the measured equilibrium constant at a given temperature is combined with data for heats of formation and entropy: $-RT \ln K_e = \Delta H_r - T\Delta S_r$. The entropy of $HO_2$ has been calculated by using the improved rotational constants given by Saito.[20] The result $S°_{298}(HO_2) = 54.73$ eu is about 0.35 eu larger than the value given in the current JANAF tables; therefore corrected $S°$ data are used in all subsequent calculations. From the value $K_e(700\ K) = 19.7$, one obtains $\Delta H_f°_{298}(HO_2) = 2.4$ kcal mol$^{-1}$ by using either JANAF or TPIS reference data. Similarly, using $K_e(500\ K) = 154$ and $K_e(1100\ K) = 3.05$, one obtains $\Delta H°_{298}(HO_2) = 2.5$ and 2.0 kcal mol$^{-1}$, respectively. The calculated temperature dependence of the $\Delta H_f(HO_2)$ is used to correct the values to the 298 K standard state.

To derive a preferred value for $\Delta H_f°(HO_2)$ from the equilibrium constant data in Figure 5, we have compared the measured temperature dependence of $K_e$ to the calculated temperature dependence of $K_e$ by using both JANAF and TPIS reference data tables. In these calculations $\Delta H_f°_{298}(HO_2)$ was varied from 2 to 3 kcal mol$^{-1}$, the limits indicated by the preliminary analyses described above. The fits given by the preferred value $\Delta H_f°_{298} = 2.5$ kcal mol$^{-1}$ are shown in Figure 5. The uncertainty limits ±0.5 kcal

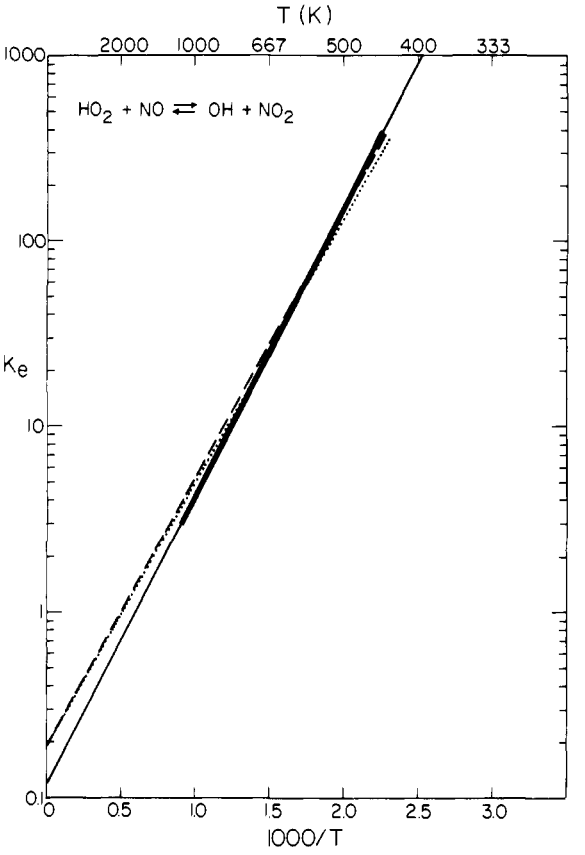


**Figure 5.** A van't Hoff plot for the equilibrium $HO_2 + NO \rightleftarrows OH + NO_2$. $K_e = k_F/k_R$ derived from Figures 2 and 4. The heavy solid line indicates the temperature range for which the measured function $K_e = (0.116 \pm 0.026) \exp[(7145 \pm 255)/RT]$ is valid. The dashed line indicates the calculated values of $K_e$ given by JANAF[4] data and $\Delta H_f°_{298}(HO_2) = 2.5$ kcal mol$^{-1}$. The dotted line indicates the calculated values of $K_e$ given by TPIS[19] data and $\Delta H_f°_{298}(HO_2) = 2.5$ kcal mol$^{-1}$.

mol$^{-1}$ include the extremes given by fitting to the high- and low-temperature ends of the $K_e$ data.

Extrapolation of the three $K_e$ data sets shown in Figure 5 to $T^{-1} = 0$ indicates that there is a descrepancy between the intercept derived from the measurements (0.116 ± 0.026) and the thermochemical data (≃0.19). The intercept is defined by the ratio of the Arrhenius preexponential $A$ factors for the forward and reverse reactions for the observed data and by the extrapolated $\Delta S_r$ for the calculated data. Thus, $A(HO_2 + NO)/A(OH + NO_2) = \exp(\Delta S_r/R)$. The difference between the observed and calculated values of $\Delta S_r$ is about 1 eu, which is too large to be attributed to an error in the thermochemical data. However, it is consistent with the uncertainty in the kinetic data when compared with the errors in the measured $A$ factors and the activation energies. Most of the uncertainty in the $K_e$ measurement is derived from the reverse rate constant ($k_R$, OH + $NO_2$) data. Because of the smaller temperature dependence and the larger temperature range of the measurements, the forward reaction Arrhenius parameters are less uncertain. To compensate for the discrepancy between the observed and calculated data in Figure 5 with the Arrhenius $A$ factor for $k_R$, we should decrease it about 40% to $\simeq 1.8 \times 10^{-11}$.

The tabulated heats of formation of NO, $NO_2$, and OH, which provide the basis for obtaining the $\Delta H_f°(HO_2)$ from the kinetic data, introduce a significant uncertainty in the final evaluation. JANAF[4] lists the uncertainties in $\Delta H_f°_{298}$ as ±0.04, ±0.2, and ±0.29 kcal mol$^{-1}$ for NO, $NO_2$, and OH, respectively. Including these values in the error analysis[21] gives a total uncertainty of ±0.6 kcal mol$^{-1}$ in the measured $\Delta H_f°_{298}(HO_2)$.

(19) Gurvich, L. V.; Veits, I. V.; Medvedev, V. A.; et al. "Thermodynamic Properties of Individual Substances"; Nauk Publishing House: Moscow, USSR, 1978; Vol. 1, pp 37, 43, 212, 216.

(20) Saito, S. *J. Mol. Spectrosc.* **1977**, *65*, 229–238.

(21) The standard method for treating propagation of random errors is to take the square root of the sum of the squares: Cvetanovic, R. J.; Singleton, D. L.; Paraskevopoulos, G. *J. Phys. Chem.* **1979**, *83*, 50–60.

Table III. Revised Thermochemical Data for the $HO_2$ Radical

| T, K | $S°$, cal $K^{-1}$ $mol^{-1}$ | $\Delta H_f°$, kcal $mol^{-1}$ |
|---|---|---|
| 0 | 0 | 3.2 |
| 298 | 54.73 | 2.5 |
| 400 | 57.26 | 2.3 |
| 500 | 59.31 | 2.1 |
| 700 | 62.66 | 1.9 |
| 1000 | 66.55 | 1.7 |

Calculated values of $S°$ and $\Delta H_f°$ for $HO_2$ at several temperatures are given in Table III.

## 4. Discussion

There are few previous measurements of the temperature dependence of the $HO_2 + NO$ and $OH + NO_2$ reaction rate constants with which the present results can be compared. Earlier work on $HO_2 + NO$ is reviewed in a recent publication.[8] The agreement of the present high-temperature measurements with previous work is excellent.

Glänzer and Troe[22] used thermal dissociation of $HNO_3$ in a shock tube to produce OH radicals and UV absorption to monitor $HNO_3$, $NO_2$, and $HO_2$ concentrations. They reported 11 kinetic measurements of the $OH + NO_2$ reaction rate constant, covering the range $1340 < T < 1760$ K. Their analysis required a correction for several competing and secondary reactions, including $HO_2 + NO_2$ and $HO_2 + OH$ for which the rate constants are not well-known at the temperatures of their measurements. The range of their measurements is shown by the shaded area in Figure 4. Their results fit the Arrhenius expression: $k_R(T) \simeq 3 \times 10^{-11} \exp[-5000/T]$ $cm^3$ $molecule^{-1}$ $s^{-1}$, which agrees very well with the present preexponential factor but rather poorly with the activation energy. The rate constants of Glänzer and Troe are a factor of 2–2.5 lower than those predicted by an extrapolation of the present measurements. Using a midrange value of $k_R$ from their work, $k_R(T = 1500\ K) \simeq 1.5 \times 10^{-12}$ $cm^3$ $molecule^{-1}$ $s^{-1}$, an estimate from this work $k_F(T = 1500\ K) \simeq 4.1 \times 10^{-2}$, and a third-law calculation, one obtains $\Delta H_f°_{298}(HO_2) \simeq 3.7$ kcal $mol^{-1}$.

There are two previous measurements of $\Delta H_f°_{298}(HO_2)$ with which the present result should be compared, Foner and Hudson[5] ($5 \pm 2$ kcal $mol^{-1}$) and Kochubei and Moin[6] ($0.9 \pm 0.6$ kcal $mol^{-1}$). Foner and Hudson obtain $\Delta H_f°(HO_2)$ from separate measurements of the electron-impact $HO_2^+$ appearance potential

$$H_2O_2 + e^- \rightarrow HO_2^+ + H + 2e^- \quad (6)$$

$AP(HO_2^+) = 15.36 \pm 0.05$ eV and the $HO_2$ ionization potential

$$HO_2 + e^- \rightarrow HO_2^+ + 2e^- \quad (7)$$

$IP(HO_2) = 11.53 \pm 0.02$ eV. The difference, (6) − (7), gives the $\Delta H$ for reaction 8: $\Delta H(8) = 88.3$ kcal $mol^{-1}$, and $\Delta H_f°(HO_2)$

$$H_2O_2 \rightarrow HO_2 + H \quad (8)$$

is calculated from the well-established heats of formation of $H_2O_2$ and H. In their analysis Foner and Hudson assume that at the observed threshold energy of (7), the fragments separate with zero kinetic and internal energies. Therefore, they calculate $\Delta H_f°(HO_2)$ by using 0 K for the reference temperature. If one uses 298 K for the reference temperature, $\Delta H_f°_{298}(HO_2) = 3.7$ kcal $mol^{-1}$. The most probable source of error in their measurement is that the fragments from (6) do possess some energy; thus as they point out, $\Delta H_f°_{298} \leq 5$ kcal $mol^{-1}$. This conclusion is consistent with the present work.

The $\Delta H_f°(HO_2)$ measurement of Kochubei and Moin[6] is based on kinetic data for the H atom abstraction reactions of $O_2$ with HCl, HBr, and HI. They assume that the activation energy, with a small correction,[23] is the endothermicity of the reaction. They have no data for the reverse reactions, and none is available for their temperature dependence. However, several measurements of the rate constant for eq 9 give $k_9(300\ K) \simeq 4.5 \times 10^{-11}$ $cm^3$

$$Cl + HO_2 \rightarrow HCl + O_2 \quad (9)$$

$molecule^{-1}$ $s^{-1}$.[24] The temperature dependence of $k_9$ is probably small, $k_9 \propto \exp[\pm 300/T]$. A third-law analysis using $k(HCl + O_2) = 8 \times 10^{-12} \exp[51500/RT]$ $cm^3$ $molecule^{-1}$ $s^{-1}$,[6] $k_9 = 4.5 \times 10^{-11}$, and JANAF data gives $\Delta H_f°_{298}(HO_2) = 4.6$ kcal $mol^{-1}$. Although Kochubei and Moin argue that independent data for the reactions of $O_2$ with HCl, HBr, and HI all lead to the same $\Delta H_f°(HO_2)$, the uncertainty in their value from unknown reverse reaction kinetics and possible secondary reactions is at least ±2 kcal $mol^{-1}$.

There are two other recent kinetic studies that also relate to $\Delta H_f°_{298}(HO_2)$. Leu and Lin[25] have reported the rate constant $k_{10} \geq 5.9 \times 10^{-12}$ $cm^3$ $molecule^{-1}$ $s^{-1}$ for eq 10. Watson[26] uses

$$OH + ClO \rightarrow HO_2 + Cl \quad (10)$$

this value and the limit given by Burrows et al.[27] for the reverse reaction $k_4 \leq 3 \times 10^{-13}$ $cm^3$ $molecule^{-1}$ $s^{-1}$ to estimate $\Delta H_f°_{298}(HO_2) \leq 1.8$ kcal $mol^{-1}$. This limit compared with the present work indicates a possible inconsistency, the origin of which is not evident at present.

Several useful thermodynamic quantities[3] derived from $\Delta H_f°(HO_2)$ are given in Table IV for 0 and 298 K. The ionization potential of $HO_2$ is calculated from the recent measurement by McCulloh[28] of the photoionization appearance potential of $HO_2^+$ from $H_2O_2$. The $IP(HO_2)$ in Table IV is $11.40 \pm 0.04$ eV compared to $11.53 \pm 0.02$ eV reported by Foner and Hudson.[5] The $\Delta H_f°_{298}(HO_2NO_2)$ is calculated from the temperature dependence of rate constant for reaction 11 reported by several workers,[29-31] $E_A = 21$ kcal $mol^{-1}$, and an estimate of the temperature dependence of the reverse reaction $E_A \simeq -1.7$ kcal $mol^{-1}$.

$$HO_2NO_2 + M \rightarrow HO_2 + NO_2 + M \quad (11)$$

The measured $\Delta H_f°(HO_2)$ establishes the thermochemistry of reactions 2–4 discussed above. At 298 K, only (2) is exothermic; $\Delta H = -0.3$ kcal $mol^{-1}$. Reactions 3 and 4 are endothermic by about 3.7 and 2.2 kcal $mol^{-1}$, respectively, and neither reaction has been observed.

Table IV. Calculated $\Delta H°$ Values Derived from $\Delta H_f°(HO_2)$ in kcal $mol^{-1}$

| | 0 K | 298 K |
|---|---|---|
| $D(HO_2\text{-}H)$ | 85.8 ± 0.6 | 87.1 ± 0.6 |
| $D(H\text{-}O_2)$ | 48.4 ± 0.6 | 49.6 ± 0.6 |
| $D(HO\text{-}O)$ | 65.1 ± 0.6 | 66.4 ± 0.6 |
| $IP(HO_2)$ | 262.8 ± 0.8 | 264.3 ± 0.8 |
| $\Delta H_f°(HO_2NO_2)$ | | −12.3 ± 2 |

**Acknowledgment.** I am grateful for valuable advice and reference information supplied by Dr. D. Wagman. This work was supported in part by the Chemical Manufacturers Association Technical Panel on Fluorocarbon Research.

(22) Glänzer, K.; Troe, J. *Ber. Bunsenges, Phys. Chem.* **1975**, *79*, 465–469.

(23) D. Wagman (private communication) has pointed out that the small correction applied by Kochubei and Moin[6] is incorrect. His reanalysis of their results gives $\Delta H_f°_{298}(HO_2) = 0.5$ kcal $mol^{-1}$.

(24) DeMore, W. B., Ed. *JPL Publ.* **1979**, *No. 79*-27, p 28.

(25) Leu, M.-T.; Lin, C.-L. *Geophys. Res. Lett.* **1979**, *6*, 425–428.

(26) Watson, R. T. "Laboratory Studies of Halogen Compounds of Atmospheric Interest", paper presented at NATO Advanced Study Institute on Stratospheric Ozone, Algarve, Portugal, Sept 30–Oct 13, 1979.

(27) Burrows, J. P.; Cliff, D. I.; Harris, G. W.; Thrush, B. A.; Wilkinson, J. P. T. *Proc. R. Soc. London, Ser. A* **1979**, *368*, 463–481.

(28) McCulloh, K., private communication. Photoionization appearance potential of $HO_2^+$ from $H_2O_2$ is reported to be $15.12 \pm 0.02$ eV at 0 K. From this one obtains $\Delta H_f°_0(HO_2^+) = 266.0 \pm 0.5$ kcal $mol^{-1}$.

(29) Graham, R. A.; Winer, A. M.; Pitts, J. N., Jr. *J. Chem. Phys.* **1978**, *68*, 4505–4510.

(30) Uselman, W. M.; Levine, S. Z.; Chan, W. H.; Calvert, J. G.; Shaw, J. H. *Chem. Phys. Lett.* **1978**, *58*, 437–440.

(31) Cox, R. A.; Patrick, K. *Int. J. Chem. Kinet.* **1979**, *11*, 635–648.